Collisionally Inhomogeneous Bose-Einstein Condensates with a Linear Interaction Gradient

Andrea Di Carli, Grant Henderson, Stuart Flannigan, Craig D. Colquhoun, Matthew Mitchell, Gian-Luca Oppo, Andrew J. Daley, Stefan Kuhr, and Elmar Haller
Department of Physics and SUPA, University of Strathclyde, Glasgow G4 0NG, United Kingdom

(Received 24 August 2019; accepted 23 September 2020; published 28 October 2020)

We study the evolution of a collisionally inhomogeneous matter wave in a spatial gradient of the interaction strength. Starting with a Bose-Einstein condensate with weak repulsive interactions in quasi-one-dimensional geometry, we monitor the evolution of a matter wave that simultaneously extends into spatial regions with attractive and repulsive interactions. We observe the formation and the decay of solitonlike density peaks, counterpropagating self-interfering wave packets, and the creation of cascades of solitons. The matter-wave dynamics is well reproduced in numerical simulations based on the nonpolynomial Schrödinger equation with three-body loss, allowing us to better understand the underlying behavior based on a wavelet transformation. Our analysis provides new understanding of collapse processes for solitons, and opens interesting connections to other nonlinear instabilities.

DOI: 10.1103/PhysRevLett.125.183602

Collisionally inhomogeneous fluids exhibit spatially varying interactions between their particles. They frequently occur at interfaces, where interaction properties change due to a variation of an external potential or due to a change of the fluid's composition. Examples for fluids at interfaces with a collisional inhomogeneity are liquid-vapor surfaces, and material junctions in condensed-matter physics. Studying quantum gases at boundaries is a current experimental challenge, with the goal to simulate mechanisms that modify transport, such as Andreev-like reflections for a gas of electrons [1,2].

In this Letter, we provide a first experimental study of the dynamical properties of a quantum gas with a *linear* collisional inhomogeneity. Specifically, we explore Bose-Einstein condensates (BEC) with spatially mixed interactions, i.e., wave packets that expand simultaneously into regions with attractive and repulsive interaction. Starting from a trapped BEC in a region with weak repulsive interaction, we monitor its spreading along a vertical guiding potential into a region with attractive interactions. We study the density profile of the wave packet as it evolves and expands, and we observe the formation and decay of a solitonlike peak, counterpropagating self-interfering wave packets, and cascades of solitons. Modeling quantitatively the underlying nonlinear dynamics numerically, we use wavelet transformations to extract position and momentum information. This allows us to understand the collapse dynamics, and identify the vital role three-body processes play in controlling these processes in experiments. This opens intriguing potential connections to related phenomena, including a recent experimental study [3] showing shock waves and soliton trains as a result of an effective negative mass in spin-orbit-coupled BECs, in which the existence of counterpropagating wave packets was also predicted [4].

Several methods were previously proposed to create quantum gases with position-dependent interactions. Optical Feshbach resonances [5–7], and optically controlled magnetic Feshbach resonances [8,9], can be used to tune the interaction strength with position-dependent properties of laser beams [9–12]. However, optical control methods are typically aimed to change the interaction strength on short length scales, and they often suffer from loss and heating of the gas. Our scheme is based on magnetic Feshbach resonances and magnetic field gradients as proposed in Refs. [13–16]. It allows for a long observation time of hundreds of milliseconds, which is necessary to study the impact of small, spatial changes of the interaction strength on the dynamical evolution of gas. We apply a magnetic field gradient $\partial_z B$ along the z direction, $B(z) = B_{\mathrm{off}} + \partial_z B z$, which directly maps the field-dependent s-wave scattering length $a(B)$ to position space. A drawback of this scheme is the creation of a strong, constant force due to the field gradient and the resulting Zeeman shift of the atomic energy levels. In our experimental setup, we apply a vertical magnetic field gradient with a value that compensates the gravitational acceleration, thus effectively canceling both forces.

Depending on the structure of magnetic Feshbach resonances, the resulting position-dependent scattering length $a(z)$ can be a complicated function showing spatial regions with attractive, repulsive, and diverging interaction. While $\partial_z B$ is determined by our levitation scheme, we can use B_{off} to control the spatial variation of $a(z)$. For a first

experimental study, we chose a regime with a linear variation of the scattering length, $a(z) = a_{\mathrm{off}} + \partial_z a z$, with a constant spatial gradient $\partial_z a$, and an offset value a_{off} at the center of the cloud at $z = 0$. The gradient introduces a new length scale to the system, $L_a = |a_{\mathrm{off}}/\partial_z a|$, which corresponds to the distance between the center of the cloud and the position of the zero crossing of $a(z)$. This length scale L_a can be compared to typical length scales of the matter-wave packet L_w, such as the Thomas-Fermi radius of a BEC or the size of a soliton. For $L_a \gg L_w$, the relative change of a is small over the extent of the matter wave, and a propagating wave packet can adapt its size and peak density while preserving its overall shape. For this regime, an analytical solution for a bright soliton was derived based on the perturbed nonlinear Schrödinger equation [13,14]. For a strong interaction gradient with $L_a \leq L_w$, the shape of the matter wave is changed and local self-amplifying feedback effects can be expected.

Details of our experimental apparatus and cooling sequence can be found in earlier publications [17,18]. A BEC of approximately 12 000 cesium atoms [18] in the Zeeman substate $|F = 3, m_F = 3\rangle$ is trapped in the dipole potential of two crossed laser beams, L_H and L_V, with trap frequencies $\omega_{x,y,z} = 2\pi \times [40(1), 40(1), 5.3(1)]$ Hz [Fig. 1(a)]. Two pairs of vertical coils create a homogeneous magnetic field B_{off} and a magnetic field gradient $\partial_z B_{\mathrm{lev}} = 31.1$ G/cm to compensate the gravitational acceleration. The scattering length a_{off} at the initial position of the BEC is $+4a_0$ with an approximately linear variation $\partial_z a = 0.21 a_0/\mu$m [Fig. 1(b)], where a_0 is Bohr's radius. We initialize the expansion of the BEC along the guiding laser beam L_V by switching off the beam L_H within 4 ms.

Figure 1(c) shows absorption images of the expanding BEC over an evolution time t of 300 ms with the corresponding horizontally integrated one-dimensional density profiles in Figs. 1(d)–1(g). To facilitate the discussion, we divide the evolution of the spreading wave packet into four phases (I–IV). Phase I is dominated by an asymmetric, interaction-driven expansion of the BEC [Fig. 1(d)]. In phase II, a sharp matter-wave front develops in the density profile on the attractive side forming a sharp solitonlike peak [Fig. 1(e)]. Periodic ripples in the density profile start to propagate from the attractive side of the wave packet to the repulsive side when the peak reaches maximum height [phase III, symbol A at 160 ms in Fig. 1(c)] and then starts to decay. At 200 ms (symbol B), only a small cloud of atoms remains where the peak was located and continues to propagate downward. A second (symbol C) and a third (symbol D) solitonlike peak are visible at 220 and 300 ms. The process of formation and decay of density peaks continues in phase IV [Fig. 1(g)], e.g., with the decay of the second peak (symbol E at 300 ms). We discuss these four phases successively in the following paragraphs.

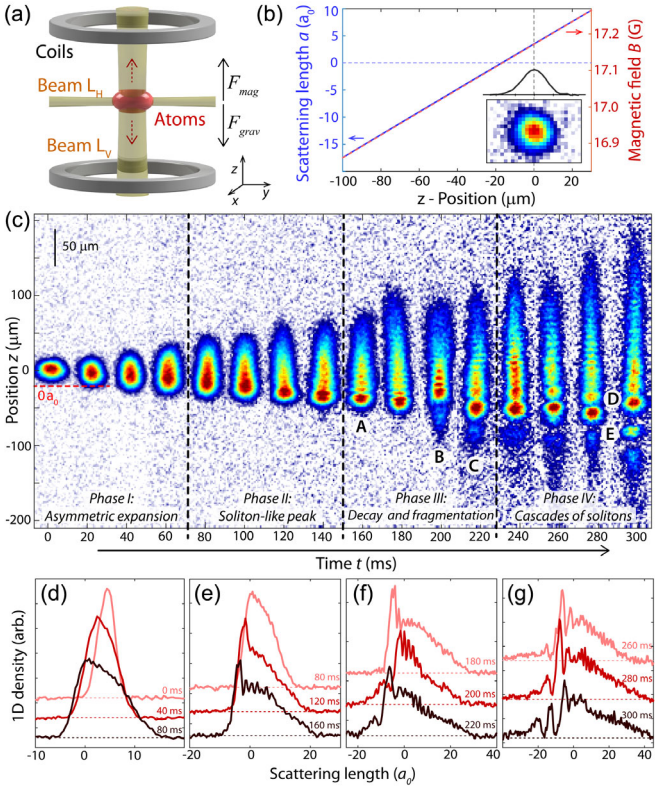

FIG. 1. (a) Experimental setup with coils and with the vertical and horizontal laser beams L_V and L_H. The gravitational force, F_{grav}, is canceled by the magnetic force F_{mag}. (b) Position dependence of the scattering length (left axis) and the magnetic field (right axis). Inset: absorption image of the initial density distribution at position $z = 0$ μm after a free expansion time of 25 ms. (c) Absorption images of the density distribution after a variable evolution time t and an expansion time of 25 ms. The color map of each image is rescaled using the peak density to enhance the visibility of the evolving structures in the density profiles. (d)–(g) Horizontally integrated density profiles of the images in (c).

Phase I. Asymmetric expansion.—Our scattering length gradient causes a linear coupling constant $g(z) = g_{\mathrm{off}} + \partial_z g z$ with an offset $g_{\mathrm{off}} = 2\hbar\omega_r a_{\mathrm{off}}$ and a gradient $\partial_z g = 2\hbar\omega_r \partial_z a$. Here, ω_r is the radial trap frequency of L_V in the horizontal plane. For small gradients with $L_a \gg L_w$ and repulsive interactions, the density profile of the ground state in the Thomas-Fermi approximation is given by

$$n(z) = \max[0, \tilde{n}(z)], \quad \tilde{n}(z) = \frac{\mu - V(z)}{g_{\mathrm{off}}}\left(1 + \frac{\partial_z a}{a_{\mathrm{off}}} z\right)^{-1}, \quad (1)$$

with an external potential $V(z)$ and a chemical potential μ. The interaction gradient adds a position-dependent scaling factor to the density profile, which, as a result, shows a shift of the peak position and a slant toward the side with smaller scattering lengths [Fig. 2(a), red lines].

The slanted density profile of the ground state results in an asymmetric expansion when we remove the vertical

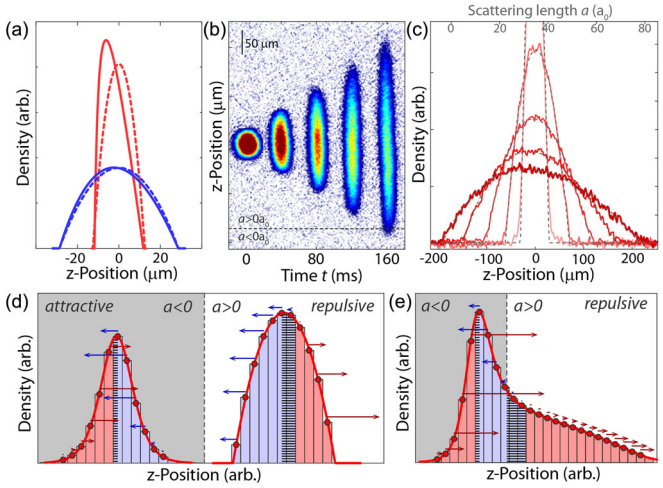

FIG. 2. (a) Calculated density profile of the ground state for $N = 13\,000$, $\omega_r = 2\pi \times 40$ Hz, $\omega_z = 2\pi \times 5.2$ Hz, $a = 3a_0$ (red) and $a_{\mathrm{off}} = 36a_0$ (blue) with $\partial_z a = 0.21a_0/\mu$m (solid lines) and $\partial_z a = 0a_0/\mu$m (dashed lines). (b) Absorption images and (c) 1D-density profiles of a BEC for varying hold times t and a constant free expansion time of 20 ms. a_{off} is $36a_0$ at the initial position of BEC. (d) Illustration of forces on sections of a BEC and soliton, and (e) during the expansion into regions with attractive interaction. Red (blue) patches and arrows indicate sections of the matter wave that are pushed toward smaller (larger) scattering length.

confinement. However, a slant can also develop in the expansion profile for a symmetric ground state wave function. We observe this effect in an expansion measurement for repulsive interaction with a larger scattering length [$a_{\mathrm{off}} = 36a_0$, Fig. 2(b)] and an almost symmetric initial wave function of the ground state [Fig. 2(a), blue line]. The expansion is driven by the conversion of interaction energy to kinetic energy [19], with an asymmetry due to the position-dependent interaction. We find excellent agreement of the density profiles [Fig. 2(c), red lines] with Eq. (1) [Fig. 2(c), gray dashed lines] assuming a shape preserving expansion [20].

Phase II. Solitonlike peak.—In addition to the asymmetric expansion, a further deceleration of the atoms occurs when the wave packet crosses the point of zero interaction [80 ms, Fig. 1(e)] and forms a sharp matter-wave front, similar to a single soliton. Here, we provide an intuitive explanation for the coherent formation of the single solitonlike peak. A full numerical simulation of the time evolution is presented when discussing phase III.

When neglecting the kinetic energy in the 1D-GPE, the force F on a section of the wave packet at position z is proportional to the spatial derivative of the interaction energy $n(z)g(z)$ with

$$F \sim -\partial_z n(z) g(z) - n(z)\partial_z g. \tag{2}$$

The first term in Eq. (2), depending on the density gradient $\partial_z n(z)$, causes the spreading of the wave packet for repulsive interaction and a contraction for attractive interaction. The second term, which depends on our interaction gradient, always accelerates the wave packet toward smaller scattering lengths. As a result, the forces are not spatially symmetric, but push the section in the middle of each wave packet toward smaller scattering lengths [Fig. 2(d), hatched areas]. Patch colors and arrows indicate the forces acting on different sections of the wave packet in Fig. 2(d) as prescribed by Eq. (2). A solitonlike peak forms when a wave packet spreads into the region with attractive interaction [Fig. 2(e)], because forces on sections with an increasing density gradient change sign and counteract the expansion, while the second term in Eq. (2) continues to push atoms toward smaller scattering lengths [Fig. 2(e), hatched areas].

Bright matter-wave solitons have been created by seeding modulational instabilities in a dense background gas with noise or interferences [26–28], and by shaping the density profile with an external potential before an interaction quench [18,29–31]. Here, in contrast, the single solitonlike peak emerges due to the propagation of the matter wave in the linear interaction gradient and without the need of additional seedings or quenches.

Phase III. Decay and fragmentation of the solitonlike peak.—The solitonlike peak propagates toward regions with stronger attractive interaction, while growing in height and shrinking in size as predicted in Ref. [13]. At approximately $t = 160$ ms [Fig. 1(c)], periodic ripples appear in the density distribution and extend, with a counterpropagating flow, into the region of repulsive interaction. The solitonlike peak has almost fully decayed at approximately $t = 200$ ms with a small cloud of atoms appearing below its former position. We employ numerical calculations based on the nonpolynomial Schrödinger equation (NPSE) [20,32] to simulate the complete evolution of the matter waves (Fig. 3). The NPSE alone with a linear dependence of the scattering length reproduces the expansion and solitonlike peak formation well in phases I and II. When the local density becomes large, it is necessary to include a three-body loss term in the model [33–36].

In the simulation, the peak density of the propagating soliton increases due to a shrinking of its width [Fig. 3(a)], until the three-body loss term increases and prevents a rapid collapse of the soliton [35,36]. To analyze the effect of the soliton's subsequent decay, we employ a Gabor wavelet decomposition of the wave function [20] similar to what was used in Ref. [4]. In contrast to a Fourier spectrum which uses delocalized sine and cosine functions, the wavelet decomposition provides information about the location, direction, and velocity of motion of wave packets at a given time. In the wavelet decomposition at $t = 150$ ms the soliton is visible as a peak in the region of attractive interactions [arrow in Fig. 3(b)]. After the soliton starts to decay at $t = 190$ ms, a counterpropagating wave packet

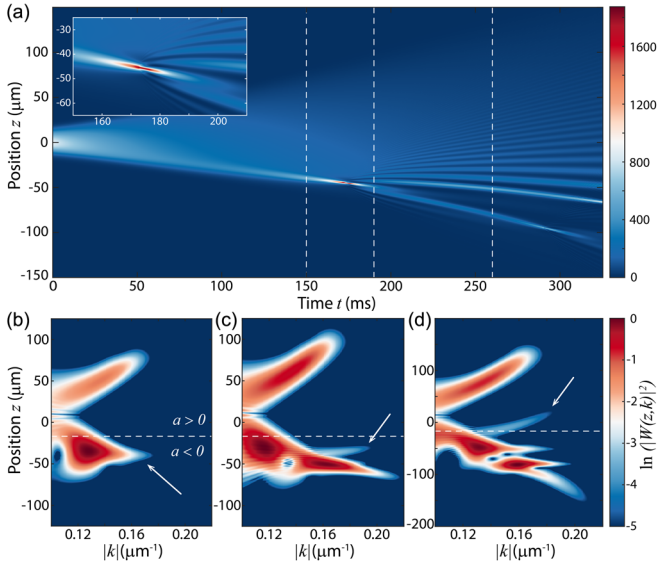

FIG. 3. (a) Numerical simulation of the evolution of the density profile using NPSE with three-body loss (1D density in atoms/μm). Inset: Zoomed region of the growing and then decaying soliton. (b) Wavelet decomposition [20] of the atomic wave function at $t = 150$ ms [first vertical line in (a)], showing the emerging soliton (white arrow). (c) Wavelet decomposition at $t = 190$ ms [second vertical line in (a)], after the appearance of the density ripples. The arrow indicates the counterpropagating wave packet. (d) Wavelet decomposition at $t = 260$ ms [third vertical line in (a)], after the counterpropagating wave packet identified by the arrow penetrates the region of repulsive interactions ($a > 0$).

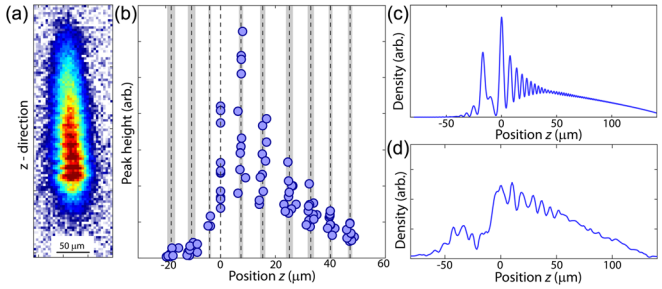

FIG. 4. Ripple pattern in the density profile for approximately 22000 atoms. (a) Absorption image of density profile after a free expansion time of 25 ms. (b) Positions of density peaks for multiple absorption images. Mean position and standard deviation of the numbered peaks are indicated by dashed lines and by gray areas, respectively. (c) Simulated density distribution at $\Delta T = 40$ ms after the decay of the soliton. (d) Measured density distribution at $\Delta T = 40$ ms [20].

develops on the side of the soliton [arrow in Fig. 3(c) at $t = 190$ ms] and then penetrates the region of repulsive interactions [arrow in Fig. 3(d) at $t = 210$ ms]. We interpret this wave packet as a partial reflection of the incoming atoms on the sharp edges of the now decaying soliton. The counterpropagating wave packet coherently interferes with the atoms moving toward negative scattering lengths, giving rise to the ripple pattern in the atomic density observed in both the attractive and repulsive interaction regions. We observe no change of the ripple pattern at the zero crossing of the scattering length, where the interaction-dependent speed of sound in the gas vanishes [dashed lines in Figs. 3(b)–3(d)].

In Fig. 4, we study the ripples of the density profile in the experiment and in the simulation. We find qualitative agreement between the density profiles of the simulation and the experiment [Figs. 4(c) and 4(d)]. In the experiment, the pattern shows fluctuations of the peak density and of the positions of the ripples, but the distances between the ripples are maintained from shot to shot. To test this, we identify for each absorption image the peak positions relative to the position of the first large density peak next to the decaying soliton [Fig. 4(b)]. The distances between the peaks are close to 8 μm, with a slow increase in time (see details in [20]).

Phase IV. Cascades of solitonlike peaks.—In the simulation, we observe that ripples in the region of repulsive interaction do not grow with propagation time and their amplitudes decay the further away they are from the point of zero scattering length. This is markedly different from atoms in regions of attractive interaction, where experiment and simulations show the formation of additional solitonlike peaks for long hold times. The peak-formation process of phase II repeats itself as atoms are continuously pushed toward the region with attractive interaction, and, for large initial densities, the density ripples of phase III attract the surrounding medium, shrink in size, grow in height, and form new separate solitonlike peaks [Fig. 3(a)]. This is in agreement with the appearance of a second and a third solitonlike peak in the experimental data during phases III and IV [symbols B and D, Fig. 1(c)]. We also expect secondary decays to occur, as those solitonlike peaks propagate toward stronger attractive interaction, and new ripple patterns form [Fig. 3(a)]. A related scheme to create multiple solitons was proposed in Ref. [37], based on a careful tuning of position-dependent interactions and an optical dipole trap. Our results show that even without the dipole trap, cascades of solitons form due to the interaction gradient.

In conclusion, we provided a first experimental study of the dynamical evolution of collisionally inhomogeneous matter waves with a linear interaction gradient. We observed the time evolution of a BEC in quasi-1D geometry, as it expands with repulsive iteration into non-interacting and attractive regions. Four characteristic phases were identified in the time evolution, i.e., an asymmetric expansion, the coherent formation and decay of a solitonlike peak, the generation and propagation of counterpropagating coherent waves, and the creation of cascades of solitons. Utilizing our spectrum of magnetic Feshbach resonances, we expect that our experimental method can be extended beyond a linear interaction

gradient and small scattering lengths, to study matter-wave transport in complex potentials with position-dependent loss and rapid interaction changes as they occur at boundaries and interfaces.

The data used in this publication are openly available at the University of Strathclyde KnowledgeBase [38].

We acknowledge support by the EU through "QuProCS" (GA 641277) and the ETN "ColOpt" (GA 721465), by the EPSRC Programme Grant "DesOEQ" (EP/P009565/1), and by the EPSRC New Investigator Grant No. EP/T027789/1. A. D. C. acknowledges financial support by EPSRC and SFC via the International Max Planck Partnership. G. H. acknowledges financial support by The Carnegie Trust via the Vacation Scholarship scheme.

[1] I. Safi and H. J. Schulz, Transport in an inhomogeneous interacting one-dimensional system, Phys. Rev. B **52**, R17040 (1995).
[2] A. J. Daley, P. Zoller, and B. Trauzettel, Andreev-Like Reflections with Cold Atoms, Phys. Rev. Lett. **100**, 110404 (2008).
[3] M. A. Khamehchi, K. Hossain, M. E. Mossman, Y. Zhang, Th. Busch, M. M. Forbes, and P. Engels, Negative-Mass Hydrodynamics in a Spin-Orbitcoupled Bose-Einstein Condensate, Phys. Rev. Lett. **118**, 155301 (2017).
[4] D. Colas, F. P. Laussy, and M. J. Davis, Negative-Mass Effects in Spin-Orbit Coupled Bose-Einstein Condensates, Phys. Rev. Lett. **121**, 055302 (2018).
[5] P. O. Fedichev, Y. Kagan, G. V. Shlyapnikov, and J. T. M. Walraven, Influence of Nearly Resonant Light on the Scattering Length in Low-Temperature Atomic Gases, Phys. Rev. Lett. **77**, 2913 (1996).
[6] F. K. Fatemi, K. M. Jones, and P. D. Lett, Observation of Optically Induced Feshbach Resonances in Collisions of Cold Atoms, Phys. Rev. Lett. **85**, 4462 (2000).
[7] M. Theis, G. Thalhammer, K. Winkler, M. Hellwig, G. Ruff, R. Grimm, and J. H. Denschlag, Tuning the Scattering Length with an Optically Induced Feshbach Resonance, Phys. Rev. Lett. **93**, 123001 (2004).
[8] D. M. Bauer, M. Lettner, C. Vo, G. Rempe, and S. Dürr, Control of a magnetic Feshbach resonance with laser light, Nat. Phys. **5**, 339 (2009).
[9] L. W. Clark, L.-C. Ha, C.-Y. Xu, and C. Chin, Quantum Dynamics with Spatiotemporal Control of Interactions in a Stable Bose-Einstein Condensate, Phys. Rev. Lett. **115**, 155301 (2015).
[10] R. Yamazaki, S. Taie, S. Sugawa, and Y. Takahashi, Submicron Spatial Modulation of an Interatomic Interaction in a Bose-Einstein Condensate, Phys. Rev. Lett. **105**, 050405 (2010).
[11] M. Yan, B. J. DeSalvo, B. Ramachandhran, H. Pu, and T. C. Killian, Controlling Condensate Collapse and Expansion with an Optical Feshbach Resonance, Phys. Rev. Lett. **110**, 123201 (2013).
[12] N. Arunkumar, A. Jagannathan, and J. E. Thomas, Designer Spatial Control of Interactions in Ultracold Gases, Phys. Rev. Lett. **122**, 040405 (2019).
[13] G. Theocharis, P. Schmelcher, P. G. Kevrekidis, and D. J. Frantzeskakis, Matter-wave solitons of collisionally inhomogeneous condensates, Phys. Rev. A **72**, 033614 (2005).
[14] G. Theocharis, P. Schmelcher, P. G. Kevrekidis, and D. J. Frantzeskakis, Dynamical trapping and transmission of matter-wave solitons in a collisionally inhomogeneous environment, Phys. Rev. A **74**, 053614 (2006).
[15] P. Niarchou, G. Theocharis, P. G. Kevrekidis, P. Schmelcher, and D. J. Frantzeskakis, Soliton oscillations in collisionally inhomogeneous attractive Bose-Einstein condensates, Phys. Rev. A **76**, 023615 (2007).
[16] A. S. Rodrigues, P. G. Kevrekidis, M. A. Porter, D. J. Frantzeskakis, P. Schmelcher, and A. R. Bishop, Matter-wave solitons with a periodic, piecewise-constant scattering length, Phys. Rev. A **78**, 013611 (2008).
[17] A. Di Carli, C. D. Colquhoun, S. Kuhr, and E. Haller, Interferometric measurement of micro-g acceleration with levitated atoms, New J. Phys. **21**, 053028 (2019).
[18] A. Di Carli, C. D. Colquhoun, G. Henderson, S. Flannigan, G.-L. Oppo, A. J. Daley, S. Kuhr, and E. Haller, Excitation Modes of Bright Matter-Wave Solitons, Phys. Rev. Lett. **123**, 123602 (2019).
[19] T. Kraemer, J. Herbig, M. Mark, T. Weber, C. Chin, H.-C. Nägerl, and R. Grimm, Optimized production of a cesium Bose-Einstein condensate, Appl. Phys. B **79**, 1013 (2004).
[20] See Supplemental Material at http://link.aps.org/supplemental/10.1103/PhysRevLett.125.183602 for additional information, which includes Refs. [21–25].
[21] S. Cowell, H. Heiselberg, I. E. Mazets, J. Morales, V. R. Pandharipande, and C. J. Pethick, Cold Bose Gases with Large Scattering Lengths, Phys. Rev. Lett. **88**, 210403 (2002).
[22] I. Simonovski and M. Boltežar, The norms and variances of the Gabor, Morlet and general harmonic wavelet functions, J. Sound Vibrat. **264**, 545 (2003).
[23] T. Kraemer, M. Mark, P. Waldburger, J. G. Danzl, C. Chin, B. Engeser, A. D. Lange, K. Pilch, A. Jaakkola, H. C. Nägerl, and R. Grimm, Evidence for Efimov quantum states in an ultracold gas of caesium atoms, Nature (London) **440**, 315 (2006).
[24] M. Gustavsson, E. Haller, M. J. Mark, J. G. Danzl, G. Rojas-Kopeinig, and H.-C. Nägerl, Control of Interaction-Induced Dephasing of Bloch Oscillations, Phys. Rev. Lett. **100**, 080404 (2008).
[25] M. Berninger, A. Zenesini, B. Huang, W. Harm, H.-C. Nägerl, F. Ferlaino, R. Grimm, P. S. Julienne, and J. M. Hutson, Feshbach resonances, weakly bound molecular states, and coupled-channel potentials for cesium at high magnetic fields, Phys. Rev. A **87**, 032517 (2013).
[26] L. D. Carr and J. Brand, Spontaneous Soliton Formation and Modulational Instability in Bose-Einstein Condensates, Phys. Rev. Lett. **92**, 040401 (2004).
[27] L. D. Carr and J. Brand, Pulsed atomic soliton laser, Phys. Rev. A **70**, 033607 (2004).
[28] J. H. V. Nguyen, D. Luo, and R. G. Hulet, Formation of matter-wave soliton trains by modulational instability, Science **356**, 422 (2017).
[29] L. Khaykovich, Formation of a matter-wave bright soliton, Science **296**, 1290 (2002).

[30] A. L. Marchant, T. P. Billam, T. P. Wiles, M. M. H. Yu, S. A. Gardiner, and S. L. Cornish, Controlled formation and reflection of a bright solitary matter-wave, Nat. Commun. **4**, 1865 (2013).

[31] T. Mežnaršič, T. Arh, J. Brence, J. Pišljar, K. Gosar, Ž. Gosar, R. Žitko, E. Zupanič, and P. Jeglič, Cesium bright matter-wave solitons and soliton trains, Phys. Rev. A **99**, 033625 (2019).

[32] L. Salasnich, A. Parola, and L. Reatto, Effective wave equations for the dynamics of cigar-shaped and disk-shaped Bose condensates, Phys. Rev. A **65**, 043614 (2002).

[33] L. Santos and G. V. Shlyapnikov, Collapse dynamics of trapped Bose-Einstein condensates, Phys. Rev. A **66**, 011602(R) (2002).

[34] Y. Kagan, A. E. Muryshev, and G. V. Shlyapnikov, Collapse and Bose-Einstein Condensation in a Trapped Bose Gas with Negative Scattering Length, Phys. Rev. Lett. **81**, 933 (1998).

[35] H. Saito and M. Ueda, Intermittent Implosion and Pattern Formation of Trapped Bose-Einstein Condensates with an Attractive Interaction, Phys. Rev. Lett. **86**, 1406 (2001).

[36] P. J. Everitt, M. A. Sooriyabandara, M. Guasoni, P. B. Wigley, C. H. Wei, G. D. McDonald, K. S. Hardman, P. Manju, J. D. Close, C. C. N. Kuhn, S. S. Szigeti, Y. S. Kivshar, and N. P. Robins, Observation of a modulational instability in Bose-Einstein condensates, Phys. Rev. A **96**, 041601(R) (2017).

[37] M. I. Rodas-Verde, H. Michinel, and V. M. Pérez-García, Controllable Soliton Emission from a Bose-Einstein Condensate, Phys. Rev. Lett. **95**, 153903 (2005).

[38] A. Di Carli, G. Henderson, S. Flannigan, C. D. Colquhoun, M. Mitchell, G.-L. Oppo, A. J. Daley, S. Kuhr, and E. Haller, Data for Collisionally inhomogeneous Bose-Einstein condensates with a linear interaction gradient, University of Strathclyde KnowledgeBase, https://doi.org/10.15129/290227b7-f661-49b8-83ac-ce5d9462ce93.